AD-A031 807 MASSACHUSETTS INST OF TECH CAMBRIDGE DEPT OF OCEAN E--ETC F/G 20/11
HIGHER MODAL DYNAMIC PLASTIC BEHAVIOR OF BEAMS LOADED IMPULSIVE--ETC(U)
OCT 76 N JONES, C A SOARES N00014-76-C-0195
UNCLASSIFIED 76-5 NL

1 OF 1
AD A031807

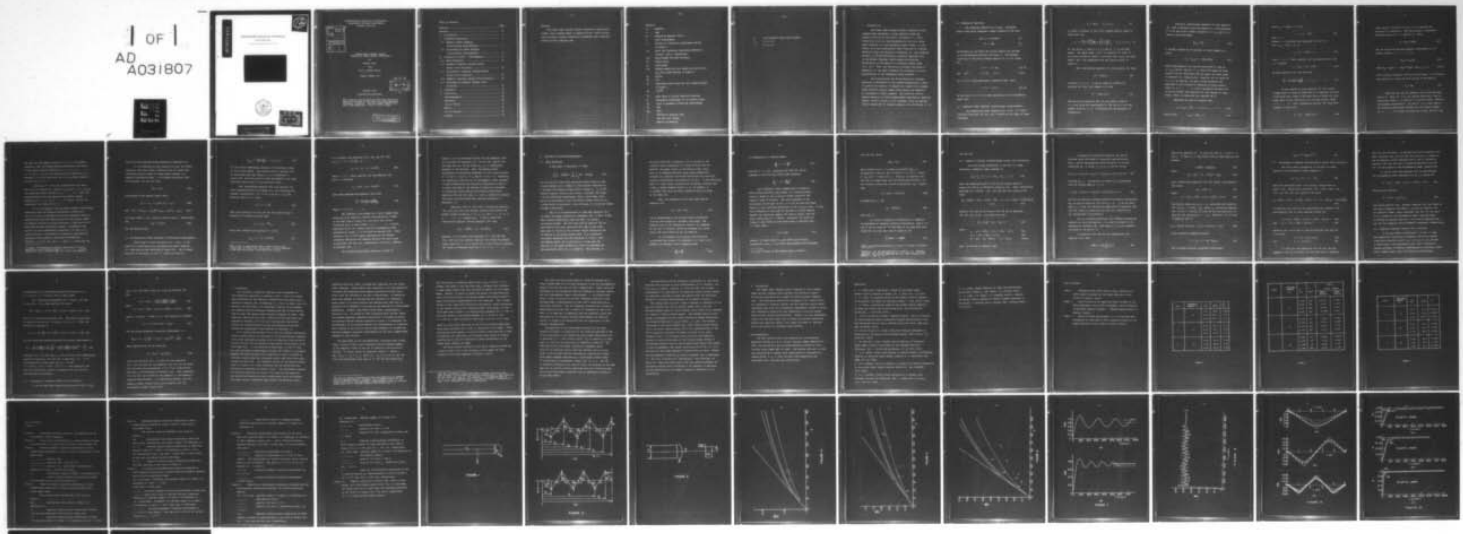

END

DATE FILMED
12-76

MASSACHUSETTS INSTITUTE OF TECHNOLOGY

Ocean Engineering

Cambridge, Massachusetts 02139

MASSACHUSETTS INSTITUTE OF TECHNOLOGY
DEPARTMENT OF OCEAN ENGINEERING
CAMBRIDGE, MASS. 02139

HIGHER MODAL DYNAMIC PLASTIC BEHAVIOR OF BEAMS LOADED IMPULSIVELY

by

Norman Jones

and

C.A.P. Guedes Soares

Report Number 76-5

October 1976

This research was carried out under the Structural Mechanics Program of the Office of Naval Research, Arlington, Virginia. Contract Number N00014-76-C-0195, Task NR064-510. M.I.T., O.S.P. 83344.

Table of Contents

Abstract.

The higher modal dynamic plastic response of impulsively loaded, fully clamped beams is examined herein, using various rigid perfectly plastic theoretical procedures and a numerical elastic-plastic computer code.

Notation

p	pressure
t	time
t^*	defined by equation (47c).
u	axial displacement
w	lateral or transverse displacement defined in Figure 1.
x,z	axial and transverse coordinates defined in Figures 1 and 3, respectively
B,H	beam breadth and beam thickness
E_r	energy ratio
$2L$	beam length
M,N	bending moment per unit length and axial force per unit length defined in Figure 3.
M_o	$\sigma_o H^2/4$
N_o	$\sigma_o H$
Q	transverse shear force per unit length defined in Figure 1.
Q_o	$\sigma_o H/\sqrt{3}$
V_o	peak value of initial impulsive velocity
W	transverse displacement at an interior hinge
W_f	final or permanent transverse displacement
W_*	W/H
W_{*f}	W_f/H
λ	defined by equation (21b)
μ	mass per unit length
ρ	density of material

σ_0	0.1% uniaxial static proof stress
$(\dot{})$	$\partial ( ) / \partial t$
$( )'$	$\partial ( ) / \partial x$

1. Introduction.

The higher modal dynamic plastic response of fully clamped beams subjected to large impulsive loads was examined recently as described in Reference [1]. Exact theoretical solutions were presented for the first three modal responses of rigid perfectly plastic beams. It was evident from some experimental tests conducted on aluminum 6061T6511 beams and reported in Reference [1] that geometry changes, or finite-deflections, played an important role in the dynamic response, which agrees with previous observations on the behavior of uniformly loaded beams (e.g. [2]). Thus, the theoretical procedure developed in Reference [3] was used to examine the influence of finite-displacements on the fundamental modal response.

The infinitesimal and finite-deflection analyses developed in Reference [1] are further generalised in order to predict the behavior of impulsively loaded, fully clamped, rigid perfectly plastic beams which undergo any symmetric or antisymmetric modal response. The numerical elastic-plastic behavior of fully clamped beams subjected to impulsive "modal" velocity fields is also examined, using the spatial finite-element *JET 3C* computer program of Wu and Witmer [4, 5].

2. Fundamental Equations.

The governing equation for a rigid perfectly plastic beam which undergoes a modal response of the form

$$\dot{w}(x, t) = \phi(x)\dot{W}(t) \tag{1}$$

is

$$M'' = -\mu\phi\ddot{W} \tag{2}$$

provided $|M| \leq M_o$ and where the various symbols are defined in the accompanying Notation and Figure 1. The boundary conditions at the fully clamped supports ($x = 0$) of a beam are

$$\phi = 0 \ , \quad M = \pm M_o \tag{3a, b}$$

and $\phi = \mp 1$, $\quad M = \pm M_o \ , \quad Q = 0 \tag{4a-c}$

at $x = L$ of a beam undergoing a symmetric mode, while

$$\phi = 0 \ , \quad M = 0 \tag{5a, b}$$

at the centre ($x = L$) of a beam responding in an antisymmetric modal form.

3.1 Symmetric Modal Response (Infinitesimal Displacements).

Any symmetrical modal response $\phi(x) = \phi(2L - x)$, which satisfies equations (3a) and (4a), consists of two types of shape functions

$$\phi_1 = \pm x/\eta_1 \quad , \quad 0 \leq x \leq \eta_1 \tag{6}$$

in region 1 adjacent to the fully clamped supports shown in Figure 2(a) and

$$\phi_i = \mp \frac{(\eta_i - x)\dot{W}_{i-1}}{(\eta_i - \eta_{i-1})\dot{W}_i} \pm \frac{(x - \eta_{i-1})}{(\eta_i - \eta_{i-1})} \quad , \quad \eta_{i-1} \leq x \leq \eta_i \tag{7}$$

for any region i, where $2 \leq i \leq n$ and $2n - 1$ is the mode number. The upper signs - and + in equation (7) refer to any region similar to region 3 in Figure 2(a), while the lower signs + and - are associated with any region similar to region 2.

Now, substituting equation (6) into equation (2) gives

$$M'' = \mp \mu \ddot{W}_1 x/\eta_1 \tag{8}$$

provided $0 \leq x \leq \eta_1$. It may be shown by integrating equation (8) twice with respect to x that

$$\ddot{W}_1 = -6M_o/(\mu \eta_1^2) \tag{9}$$

when satisfying equation (3b) for the plastic hinge at $x = 0$ and using the requirements $M = \mp M_o$ and $Q = 0$ for the plastic hinge at $x = \eta_1$ to evaluate the two constants of integration.

Similarly, substituting equation (7) into equation (2), then integrating once with respect to x and satisfying $Q = 0$ at the plastic hinges located at $x = \eta_{i-1}$ and $x = \eta_i$ leads to the requirement

$$\dot{W}_{i-1} = \dot{W}_i . \tag{10}$$

A further integration of equation (2) with respect to x gives

$$(\eta_i - \eta_{i-1})^2 = -12M_o/(\mu\ddot{W}_i) \tag{11}$$

when using equation (10) and the conditions $M = \pm M_o$ at $x = \eta_{i-1}$ and $M = \mp M_o$ at $x = \eta_i$, where the upper and lower signs of M_o are associated with the upper and lower signs in equation (7), respectively. Equation (10) is valid for $2 \leq i \leq n$ so that $\dot{W}_1 = \dot{W}_2$ when i=2 and therefore the magnitude of the velocity is identical at every plastic hinge (1, 2, 3, . . . , n) and is henceforth denoted as $\dot{W}$. It is now evident that equation (9) also applies to every hinge. Thus, no subscripts are required for $\ddot{W}$.

Equations (9) and (11) predict that

$$\eta_i = \eta_{i-1} + \sqrt{2}\eta_1 , \quad i = 2, 3, . . . , n \tag{12}$$

which gives

$$\eta_{n-1} + \sqrt{2}\eta_1 = L \tag{13}$$

since $\eta_n = L$ when $i = n$, and

$$\eta_1 = \eta_2 - \sqrt{2}\eta_1 \tag{14}$$

when $i = 2$.

However, it is evident from equations (12) and (13) that $\eta_{n-j} + j\sqrt{2}\eta_1 = L$, or

$$\eta_i + (n - i)\sqrt{2}\eta_1 = L \tag{15}$$

when $n - j = i$. Thus, equation (14) and equation (15) with $i = 2$ predict

$$\eta_1 = L/\{1 + (n - 1)\sqrt{2}\} \tag{16}$$

so that equations (15) and (16) give

$$\frac{\eta_i}{L} = \frac{1 + (i - 1)\sqrt{2}}{1 + (n - 1)\sqrt{2}}, \quad i = 1, 2, \ldots, n \tag{17}$$

It now remains to solve equation (9) for a fully clamped beam of length 2L subjected to an impulsive velocity field which has a shape of the same form as Figure 2(a) with equal peak initial velocities $|V_o|$ at every plastic hinge 1, 2, . . . , n. Thus, integrating equation (9) twice with respect to time gives

$$W = V_o t - 3M_o t^2/(\mu\eta_1^2) \tag{18}$$

when using $W = 0$ and $\dot{W} = V_o$ at $t = 0$ to evaluate the constants of integration. The beam reaches a permanently deformed profile at $t = T$ when $\dot{W} = 0$. Thus,

$$T = \mu V_o \eta_1^2/(6M_o) \tag{19}$$

and the associated maximum permanent displacement at all plastic hinges 1, 2, . . . , n, is

$$W_{*f} = \lambda \eta_{*1}^2/12 \tag{20}$$

where $W_{*f} = W_f/H$, $\lambda = \mu V_o^2 L^2/(M_o H)$, and $\eta_{*1} = \eta_1/L$ (21a-c)

with η_1 given by equation (16) for the 2n-1 mode. It is evident from equation (1) that the final profile of the beam is

$$w_f = \phi W_f \tag{22}$$

Equations (2) and (9) indicate that M" has the same sign as ϕ. Thus, $M'' > 0$ in all regions below the x axis in Figure 2(a) since $\phi > 0$, while $M'' = 0$ on the x axis. However, the boundary conditions $M = -M_o$ and $M' = Q = 0$ were used in the foregoing theoretical analysis for all plastic hinges (1, 3, . . . , n-1) which lie below the x axis, while $M = M_o$

was used for the support hinge at $x = 0$.† It is evident, therefore, that the bending moment distribution has minima at the plastic hinges located at $x = \eta_i$ ($i = 1, 3, \ldots, n - 1$) and $M > -M_o$ for all other parts of a beam with $\phi \geq 0$. Moreover, it is now clear that $-M_o \leq M \leq M_o$ within region 1 for which $0 \leq x \leq \eta_1$.

Similarly, $M'' < 0$ for all regions which lie above the x axis in Figure 2(a), while $M = M_o$ and $M' = Q = 0$ at all the associated plastic hinges ($2, 4, \ldots, n$). Thus, the bending moment field has maxima at the plastic hinges located at $x = \eta_i$ ($i = 2, 4, \ldots, n$) and $M < M_o$ for all other parts of a beam with $\phi \leq 0$.

It is now apparent that the bending moment distribution associated with the foregoing theoretical solution has $-M_o \leq M \leq M_o$ and is therefore statically admissible since it satisfies the required conditions at all the plastic hinges and nowhere violates the yield criterion in those parts of a beam lying between the plastic hinges. Furthermore, the solution is also kinematically admissible, so that it is exact according to the methods of plasticity developed for structures which undergo infinitesimal deflections. Equations (19) and (20) with $n = 1$ and $n = 2$ agree with the

---

† In fact, the theoretical analysis also caters for the possibility that plastic hinges ($2, 4, 6, \ldots, n$) lie below the x axis, in which case $M = -M_o$ at the support.

first and third mode solutions presented in Reference [1].

It is convenient at this juncture to list, for future reference, the total angular rotation rates ($\dot{\theta}$) across the individual plastic hinges in a beam which responds in a symmetric deformation mode. It is evident from Figure 2(a) and equations (10) and (12) that

$$|\dot{\theta}_0| = \dot{W}/\eta_1 \tag{23a}$$

corresponds to the support hinge, while

$$|\dot{\theta}_1| = (\eta_1 + \eta_2)\dot{W}/\{\eta_1(\eta_2 - \eta_1)\} \tag{23b}$$

and $$|\dot{\theta}_i| = 2(\eta_{i+1} - \eta_{i-1})\dot{W}/\{(\eta_{i+1} - \eta_i)(\eta_i - \eta_{i-1})\} \tag{23c}$$

for hinge number 1 and a typical interior hinge i, respectively, and

$$|\dot{\theta}_n| = |\dot{\theta}_i|/2 \tag{23d}$$

for the central hinge.

3.2 Antisymmetrical Modal Response (Infinitesimal Displacements).

Three types of shape functions $\phi(x) = -\phi(2L - x)$ are required to characterise any antisymmetrical modal response of a beam such as that indicated in Figure 2(b). Two of these are given by equations (6) and (7), while the third is

$$\phi_{n+1} = \mp \frac{(L - x)}{(L - \eta_n)} , \quad \eta_n \leq x \leq L \tag{24}$$

for the region immediately adjacent to the mid-span, where 2n is the mode number. The negative sign in equation (24) is associated with with region (n + 1) illustrated in Figure 2(b), while the positive sign corresponds to the case when the plastic hinge n lies below the x axis.

Now, substituting equation (24) into equation (2) then integrating twice with respect to x and satisfying the boundary conditions $M' = Q = 0$, $M = \pm M_o$ at $x = \eta_n$[†] and equation (5b) at $x = L$ gives

$$\eta_n = L - \eta_1/\sqrt{2} \tag{25}$$

when using equations (9) and (10) for the plastic hinge n. Equation (12) remains valid so that

$$\eta_n = \eta_{n-1} + \sqrt{2}\eta_1 , \tag{26}$$

which when combined with equation (25) gives

$$\eta_{n-1} = L - (1 + 1/2)\sqrt{2}\eta_1 . \tag{27}$$

[†]The + sign is associated with a plastic hinge n as illustrated in Figure 2(b), while the - sign corresponds to the case when hinge n lies below the x axis.

It is evident from equations (12), (26) and (27) that $\eta_{n-j} = L - (j + 1/2)\sqrt{2}\eta_1$, or

$$\eta_i = L - (n - i + 1/2)\sqrt{2}\eta_1 \tag{28}$$

when $n - j = i$. Thus, equation (14) and equation (28) with $i = 2$ predicts

$$\eta_1 = L/\{1 + (n - 1/2)\sqrt{2}\} \tag{29}$$

which when combined with equation (28) gives

$$\frac{\eta_i}{L} = \frac{1 + (i - 1)\sqrt{2}}{1 + (n - 1/2)\sqrt{2}} \tag{30}$$

where $i = 1, 2, 3, \ldots, n$.

The response is now sought for a fully clamped beam subjected to an impulsive velocity field which has a shape of the same form as Figure 2(b) with equal peak initial velocities $|V_o|$ at every hinge 1, 2, 3, . . . , n. In fact, equations (6) to (11) remain valid for antisymmetric mode deformations, except η_i is now given by equation (28). Thus, equations (18) to (22) remain unchanged and the maximum transverse deflection and response duration are again given by equations (20) and (19), respectively, but with η_1 defined by equation (29).

The foregoing theoretical solution is exact in

regions 1 to n as discussed earlier for the symmetric case. It is evident for equations (2), (9) and (24) that M" has the same sign as ϕ in the region $\eta_n \leq x \leq L$ immediately adjacent to the mid-span. Thus, the bending moment distribution is statically admissible in this region because M' = 0 and $M = \pm M_o$ at $x = \eta_n$ and M = 0 at x = L. Therefore, the theoretical solution for an antisymmetric modal response is both kinematically and statically admissible so that it is exact according to the methods of plasticity developed for structures which undergo infinitesimal deflections. Equations (19) and (20) with n = 1 and η_1 defined by equation (29) agree with the second mode solution presented in Reference [1].

Equations (23a) to (23c) with η_i defined by equation (30) again give the total angular rotation rates across the plastic hinges located at x = 0, $x = \eta_1$ and $x = \eta_i$ (i = 2, 3, 4, . . . , n - 1), respectively. It can be shown when substituting equation (30) into equation (23c) that

$$|\dot{\theta}_i| = 2\sqrt{2}\dot{w}\{1 + (n - 1/2)\sqrt{2}\}/L. \qquad (31)$$

Moreover, it is evident from equations (1), (24)-(26) and (29), that the total angular rotation rate across the plastic hinge located at $x = \eta_n$ in Figure 2(b) is also given by equation (31) which is therefore valid for i = 2, 3, 4, . . . , n.

4. Influence of Finite-Displacements.

4.1 Basic Equations.

It was shown in Reference [3] that

$$\int_A (p - \mu\ddot{w})\dot{w}dA = \sum_{i=1}^{r} \int_{C_i} (Nw - M)\dot{\theta}_i dC_i \qquad (32)$$

for an initially flat rigid perfectly plastic plate of area A which deforms into a number of rigid regions separated by r straight line plastic hinges each of length C_i. $\dot{\theta}_i$ is the relative angular rotation rate across a straight line hinge, w is the transverse displacement along a line hinge, and N and M are the membrane force and bending moment which act on a plane which is transverse to the mid-plane of a plate and passes through a line hinge.

Now, it is straightforward to show that equation (32) is simply an energy conservation statement, and, in fact, it has been recently rederived by Taya and Mura [6] using a variational method. The left hand side of equation (32) is the external work rate, while the term $-M\dot{\theta}_i$ on the right hand side is related to the internal energy dissipation due to bending at the plastic hinge lines. If w is measured vertically downwards from the mid-plane of a plate, then the bending moment (M) is positive at a hinge when the material on the upper surface of a plate is stretched and the associated value of $\dot{\theta}_i$ is negative. The term $Nw\dot{\theta}_i$ on

the right hand side of equation (32) is related to the internal energy dissipation of a plate arising from the membrane (in-plane) forces at the plastic hinge lines. This can be demonstrated when using simple geometrical arguments for moderate transverse deflections for which the in-plane displacements are assumed to be zero. In the particular case of a rigid region rotating with an angular rotation rate $\dot{\theta}$ about a simple support having $w = 0$, for example, it is evident that $w\dot{\theta}$ is the axial extension rate of a hinge at the other end.

Thus, the integrand on the right hand side of equation (32)

$$D_i = (Nw - M)\dot{\theta}_i \tag{33}$$

can be interpreted as the internal energy dissipation rate per unit length of a straight line hinge. The explicit form of the dissipation function (D_i) depends on the type of supports around the boundary of a plate and on the yield condition for the material.

If the maximum normal stress yield criterion is selected (see Figure 5 of Reference [3]) then it is evident from Figure 3 that a membrane force

$$\frac{N}{N_o} = \frac{2z}{H} \tag{34}$$

is accompanied by a bending moment

$$\frac{M}{M_o} = -1 + \frac{4z^2}{H^2} \tag{35}$$

provided $0 \leq z \leq H/2$. Equations (34) and (35) can be combined to give the well known yield condition

$$\frac{M}{M_o} = -1 + \left(\frac{N}{N_o}\right)^2 \tag{36}$$

Now, consider a fully clamped span of length 2L which remains entirely rigid except at a central plastic hinge of length 2c and at plastic hinges located at the supports, each of length c. The axial extension of the mid-surface of the span is w^2/L, or $w^2/2L$ for each half span, where w is the transverse deflection at the central hinge. If the axial extension of each half of the span is divided equally between the associated support and central hinges, then the axial strain rate is $\dot{\varepsilon} = w\dot{w}/2Lc$. Similarly, the curvature change at the hinges are w/cL which gives a curvature rate $\dot{\kappa} = \dot{w}/cL$. Thus,

$$\dot{\varepsilon}/\dot{\kappa} = w/2. \tag{37}$$

However, if plane cross-sections remain plane during deformation, then $\dot{\varepsilon} = z\dot{\kappa}$,† which when combined with equations

†z is the location of the neutral axis in Figure 3.

(34) and (37) gives

$$N/N_o = w/H \tag{38}$$

which requires $w/H \leq 1$ in order to maintain $N/N_o \leq 1$. Consequently, equation (36) is valid if $0 \leq w/H \leq 1$, while $N = N_o$ and $M = 0$ when $w/H \geq 1$. Finally, if equations (36) and (38) are substituted into the dissipation function (33) for a beam or plate with a solid cross-section ($N_o = 4M_o/H$), then

$$D_i = M_o(1 + 3w^2/H^2)\dot{\theta}_i \tag{39}*$$

provided $w/H \leq 1$, and

$$D_i = 4M_o w\dot{\theta}_i/H \tag{40}$$

when $w/H \geq 1$.

If a beam of length 2L is subjected to a symmetric or antisymmetric impulsive velocity distribution, then $p = 0$, and it can be shown for one half span of the beam with unit width that the left hand side of equation (32)

$$-\int_o^L \mu\ddot{w}\dot{w}dA = -\mu L\ddot{W}\dot{W}/3 \tag{41}$$

when $\dot{w}$ is defined by equation (1) and ϕ is given in Figures

*Equation (39) was derived for $M < 0$ and $\dot{\theta}_i > 0$. However, equation (39) is also obtained for the other possible case when $M > 0$ and $\dot{\theta}_i < 0$.

2(a) and 2(b).

4.2 Symmetric Response (Maximum Normal Stress Yield Criterion).

The total energy dissipation in one half of a beam undergoing a symmetric modal response is

$$D_T = D_o + D_1 + (n - 2)D_i + D_n , \quad n \geq 2 \tag{42}$$

where the subscripts refer to the plastic hinges shown in Figure 2(a) and D_i is defined by equation (33). Thus, substituting equations (17), (23a-d), (33), (36) and (38) into equation (42) gives

$$D_T = 2M_o\dot{W}\{1 + \sqrt{2}(n - 1)\}\left[1 + \sqrt{2}(n - 1) + \{1 + 3\sqrt{2}(n - 1)\}W^2/H^2\right]/L, \quad n \geq 2. \tag{43}$$

Equation (32) can now be written with the aid of equations (41) and (43) in the non-dimensional form

$$\ddot{W}_* + \beta_1 W_*^2 = \beta_2 , \quad W_* \leq 1 \tag{44}$$

where

$$\beta_1 = 6\{1 + 3\sqrt{2}(n - 1)\}\{1 + \sqrt{2}(n - 1)\}/\lambda \tag{45}$$

$$\beta_2 = - 6\{1 + \sqrt{2}(n - 1)\}^2/\lambda \tag{46}$$

$$W_* = W/H , \quad \ddot{W}_* = \ddot{W}H/V_o^2 , \quad t_* = tV_o/H \tag{47a-c}$$

and λ is defined by equation (21b).

A theoretical solution of equation (44) may be obtained using the method of successive approximations. Thus, a second approximation which satisfies the initial conditions $W_* = 0$ and $\dot{W}_* = 1$ at $t_* = 0$ can be written

$$W_* = t_* + \beta_2 t_*^2/2 - \beta_1 t_*^4(1 + 3\beta_2 t_*/5 + \beta_2^2 t_*^2/10)/12 \qquad (48)$$

provided $W_* \leq 1$. The duration of motion T_* is associated with the instant when $\dot{W}_* = 0$, or

$$1 + \beta_2 T_* - \beta_1 T_*^3(1 + 3\beta_2 T_*/4 + 3\beta_2^2 T_*^2/20)/3 = 0 \qquad (49)$$

and the corresponding maximum permanent transverse displacement W_{*f} is given by equation (48) with $t_* = T_*$. It can be shown when $\beta_1 = 0$ that the theoretical predictions of equations (48) and (49) reduce to equations (20) and (19), respectively, for infinitesimal displacements.

Now, as remarked previously, the foregoing theoretical solution is valid provided $W_* \leq 1$ in order to ensure $N \leq N_o$ according to equation (38). The case $W_* \geq 1$ is now examined for which $N = N_o$ and $M = 0$.

If equations (40) and (41) are substituted into equation (32), then

$$-\mu L\dddot{W}W/3 = 4M_o W \sum_{i=1}^{n} \phi\dot{\theta}_i/H \qquad (50)$$

when using equation (1). It turns out that $\dot{\theta}_i > 0$ when $\phi = 1$, and $\dot{\theta}_i < 0$ when $\phi = -1$ (see Figure 2(a)), so that equation (50) becomes

$$-\mu LWW/3 = 4M_o W\dot{\theta}_T/H \tag{51}$$

where

$$\dot{\theta}_T = |\dot{\theta}_1| + (n - 2)|\dot{\theta}_i| + |\dot{\theta}_n|. \tag{52}$$

Thus, substituting equations (17) and (23b-d) into equation (51) gives

$$\ddot{W}_* + \alpha^2 W_* = 0 \tag{53}$$

where

$$\alpha^2 = 12\{1 + \sqrt{2}(n - 1)\}\{1 + 2\sqrt{2}(n - 1)\}/\lambda. \tag{54}$$

The initial conditions at $t_* = t_{*i}$ associated with equation (53) are $W_* = 1$ and $\dot{W}_* = \dot{W}_{*i}$, where t_{*i} is given by equation (48) with $W_* = 1$ and $\dot{W}_{*i}$ is given by the time derivative of equation (48) evaluated at $t = t_{*i}$. Therefore, the solution of equation (54) is

$$W_* = (\dot{W}_{*i}/\alpha)\sin\{\alpha(t_* - t_{*i})\} + \cos\{\alpha(t_* - t_{*i})\} \tag{55}$$

which predicts a response duration

$$T_* = t_{*i} + \alpha^{-1}\tan^{-1}(\dot{W}_{*i}/\alpha) \tag{56}$$

and a maximum permanent transverse displacement

$$W_{*f} = (1 + \dot{W}_{*i}^2/\alpha^2)^{1/2} \tag{57}$$

4.3 Antisymmetric Response (Maximum Normal Stress Yield Criterion).

The total energy dissipation in one half of a beam undergoing an antisymmetric modal response is

$$D_T = D_o + D_1 + (n - 1)D_i , \tag{58}$$

where the subscripts refer to the plastic hinges shown in Figure 2(b). Substituting equations (23a), (23b), (30), (31), (33), (36) and (38) into equation (58) gives

$$D_T = M_o\dot{W}\{1 + \sqrt{2}(n - 1/2)\}\left[2 + \sqrt{2}(2n - 1) + \{2 + 3\sqrt{2}(2n - 1)\}W^2/H^2\right]/L. \tag{59}$$

If equations (41) and (59) are substituted into equation (32) then equation (44) is again obtained, except now

$$\beta_1 = 6\{1 + 3\sqrt{2}(n - 1/2)\}\{1 + \sqrt{2}(n - 1/2)\}/\lambda \tag{60}$$

and

$$\beta_2 = - 6\{1 + \sqrt{2}(n - 1/2)\}^2/\lambda. \tag{61}$$

Equation (29) can be used to rewrite equations (60) and (61) in the form

$$\beta_1 = 6(3 - 2\eta_{*1})/(\lambda\eta_{*1}^2) \tag{62}$$

and

$$\beta_2 = - 6/(\lambda\eta_{*1}^2). \tag{63}$$

It turns out that equations (45) and (46) for the symmetric case can be recast into the same form as equations

(62) and (63) provided η_1 is defined according to equation (16). Thus, equations (44) and (47)-(49) are valid for all symmetric and antisymmetric modal responses with β_1 and β_2 defined by equations (62) and (63) and η_1 defined by equations (16) and (29) for the symmetric and antisymmetric cases, respectively.

It can be shown that equation (53) is also obtained for antisymmetric modal responses with $W_* \geq 1$, except now

$$\alpha^2 = 12\{1 + \sqrt{2}(n - 1/2)\}\{1 + \sqrt{2}(2n - 1)\}/\lambda \qquad (64)$$

which can be rewritten

$$\alpha^2 = 12(2 - \eta_{*1})/(\lambda \eta_{*1}^2) \qquad (65)$$

when using equation (29). However, equation (54) also takes on the form of equation (65) when η_1 is given by equation (16) for symmetric modes. Thus, equations (56) and (57) are valid for all symmetric and antisymmetric modal responses when α is defined by equation (65) and η_1 is given by equations (16) and (29) for symmetric and antisymmetric responses, respectively.

4.4 Symmetric Response (Square Yield Criterion).

It has been shown in References [2] and [3] that the theoretical predictions of equation (32) with a square yield curve relating N and M (i.e., $N = N_o$, $M = M_o$) provide a lower bound to the experimental and "exact" theoretical maximum permanent transverse displacements of uniformly loaded fully clamped beams, while the theoretical predictions

corresponding to an inscribing square yield surface (i.e., $N = 0.618\ N_o$, $M = 0.618\ M_o$) give an upper bound.

Now, substituting equations (17), (23a-d), (41) and $N = N_o$ and $M = \pm M_o$ into equation (32) gives

$$\ddot{W}_* + \alpha^2 W_* = -\alpha^2\{1 + \sqrt{2}(n - 1)\}/\{2 + 4\sqrt{2}(n - 1)\} \ , \quad (66)$$

where α^2 is defined by equation (54). The initial conditions of equation (66) are $W_* = 0$ and $\dot{W}_* = 1$ at $t_* = 0$. Thus, the duration of response is

$$T_* = \alpha^{-1} \tan^{-1}\left[\alpha^{-1}\{2 + 4\sqrt{2}(n - 1)\}/\{1 + \sqrt{2}(n - 1)\}\right], \quad (67)$$

and the associated maximum permanent transverse displacement is

$$W_{*f} = \frac{\{1 + \sqrt{2}(n - 1)\}}{2\{1 + 2\sqrt{2}(n - 1)\}}\left[\left\{1 + \frac{\lambda\{1 + 2\sqrt{2}(n - 1)\}}{3\{1 + \sqrt{2}(n - 1)\}^3}\right\}^{1/2} - 1\right]. \quad (68)$$

Equations (67) and (68) with $n = 1$ for the first mode respectively agree with equations (35) and (34) in Reference [1]. It is straightforward to show when $\tan \alpha T_* \simeq \alpha T_*$ and $\lambda\{1 + 2\sqrt{2}(n - 1)\}\{1 + \sqrt{2}(n - 1)\}^{-3}/3 << 1$ that equations (67) and (68) respectively reduce to equations (19) and (20) for infinitesimal displacements.

4.5 Antisymmetric Response (Square Yield Criterion).

It can be shown when substituting equations (23a), (23b),

(30), (31), (41) and $N = N_o$, $M = \pm M_o$ into equation (32) that

$$\ddot{W}_* + \alpha^2 W_* = - \frac{\alpha^2\{1 + \sqrt{2}(n - 1/2)\}}{2\{1 + 2\sqrt{2}(n - 1/2)\}} \tag{69}$$

where

$$\alpha^2 = 12\{1 + \sqrt{2}(n - 1/2)\}\{1 + 2\sqrt{2}(n - 1/2)\}/\lambda \tag{70}$$

and $W_* = 0$ and $\dot{W}_* = 1$ when $t_* = 0$. The duration of response is

$$T_* = 1/\alpha \tan^{-1}\{2(2 - \eta_{*1})/\alpha\} \tag{71}$$

and the maximum permanent transverse displacement is

$$W_{*f} = (2 - \eta_{*1})^{-1}\left[\{1 + \lambda\eta_{*1}^2(2 - \eta_{*1})/3\}^{1/2} - 1\right]/2 \tag{72}$$

where equation (70) can be rewritten

$$\alpha^2 = 12(2 - \eta_{*1})/(\lambda\eta_{*1}^2) \tag{73}$$

when using equation (29). It turns out that equations (67), (68) and (54) for the symmetric case can also be recast into the same form as equations (71) to (73), respectively, provided η_1 is now defined by equation (16). Thus, equations (71) and (72) can be used for any symmetric or antisymmetric response mode provided η_1 is defined by equation (16) for symmetric modes (Figure 2(a)) and by equation (29) for antisymmetric modes (Figure 2(b)).

5. Discussion.

The influence of material elasticity was disregarded in the theoretical solutions in sections 3 and 4. This is a reasonable simplification for impulsive loadings when the energy ratio defined by equation (44) in Reference [1] is not too small [see 7,8]. Recently, Wu and Witmer [4,5] developed a spatial finite-element and temporal central-difference computer code JET 3C which can be used to study the dynamic elastic-plastic response of beams. Some numerical results for the first, second and third mode cases are compared in Figures 4 to 9 with the rigid-plastic theoretical predictions presented herein and the corresponding strain-rate insensitive experimental tests reported in Reference [1].

It is evident from Figures 4 to 6 that the simplest theoretical solution which retains the influence of finite-deflections (equation (72)) gives reasonable agreement with the numerical elastic-plastic results and with the corresponding experimental values except in the third mode case. It was observed in References [2] and [3] that the same theoretical method which retained the influence of geometry changes gave good agreement with experimental results recorded on uniformly loaded beams and rectangular plates made from strain-rate insensitive materials. The numerical values for the elastic-plastic cases in Figures 4 to 6 were estimated from the deflection-time histories as indicated in Figures 7 and 8. The experimental results for the third mode case in Figure 6 lie below all the numerical and theoretical predictions and is conceivably due to the neglect of rotary inertia, transverse shear effects and material strain

hardening which are likely to become more important for the higher modal responses. These effects were neglected in all the theoretical solutions and transverse shear effects and material strain hardening† were not retained in the JET 3C calculations. It should be noted that Symonds [9] incorporated the influence of transverse shear forces in a yield criterion and observed that they were responsible for a decrease in the slope at the mid-span of a beam loaded dynamically. However, when these results were reconsidered in Reference [10] , it turned out that transverse shear effects caused the maximum permanent transverse deflections to increase as can be interpreted from the results presented in Figure 4 of Reference [10] . Nevertheless, it is not known whether the incorporation of transverse shear effects in the yield criterion would decrease or increase the maximum permanent transverse displacements of the fully clamped beams examined in this article.

The magnitudes of the non-dimensional transverse shear forces (Q/Q_o) listed in Table 1 were estimated from the bending moments in the computer output of the JET 3C numerical elastic-plastic program. If rotary inertia is neglected, then $Q = - dM/dx = - (M_i - M_{i-1}) / (x_i - x_{i-1})$, where $(x_i - x_{i-1})$ is 0.25 in. for the first and second mode cases and 0.1 in. for the third mode case.

---

†The JET 3C computer program does have the capability to examine strain hardening effects. However, the ultimate stress for the aluminum 6061T6511 test specimens is approximately only 1.4 percent larger than the 0.1 percent offset yield stress (σ_o) [1].

The fully plastic transverse shear force is $Q_o = \sigma_o H/\sqrt{3}$. It is evident from Table 1 that the ratio Q/Q_o increases, with increase in mode number despite the fact the W_f/H is smaller for the higher modes. However, in order to reduce the amount of output data and lower the printing costs, the bending moment distribution across a beam was printed at approximately 20 μsec intervals. Thus, larger values of Q/Q_o could have occurred at intermediate times.† Furthermore if the largest value of the transverse shear force (Q/Q_o) for the third mode case in Table 1 is alternatively estimated at x = 0.25 in. using the values of the bending moments at x = 0.125 in. and x = 0.375 in., then it turns out that $Q/Q_o \simeq 0.28$ at t = 20.3 μsec which is still larger than Q/Q_o in the first and second mode cases which were calculated for a 0.25 in. separation of the modes. These observations would appear to justify further investigations in order to determine the importance of transverse shear forces on plastic yielding and to seek the influence of shear deformations on the higher modal response of beams.

The axial strains according to the JET 3C numerical method are listed in Table 2 for a few locations, on the upper and lower surfaces of the beams examined in Figures 7 and 8.

---

†The JET 3C computer program was used to repeat the third mode case in Table 1 with output printed at approximately 1 μsec intervals for the first 150 μsec of the response. It transpired that at x = 0.1 in., Q/Q_o equalled 0.41, 0.41 and 0.40 when t equalled 1.02 μsec, 16.25 μsec and 26.4 μsec, respectively.

The first and third mode classical vibration periods for a fully clamped beam with the same parameters as the one considered in Figure 8 are 596 μsec and 110 μsec, respectively. These values are predicated on the assumptions that the response is entirely elastic and the displacements remain infinitesimal. It is evident from Figure 8 that the period of the high frequency vibration of the deformed beam is approximately 85 μsec and is associated with a third mode vibration. The low frequency vibration has a period of approxiamtely 595 μsec and is related to vibrations in the first mode. It is important to emphasize that the classical values were developed for an initially straight beam whereas the numerical results in Figure 8 are associated with the vibrations of a permanently deformed beam.

The amplitude of the first modal vibration for the beam examined in Figure 8 is sensitive to the relative magnitude of the initial velocities at the center and outer hinges (See Figure 2(c) of Reference [1]). This velocity ratio (V_0 at center/V_0 at outer peak) is 1.022 for the beam which is examined in Figure 8. The amplitude of the first modal vibration is somewhat larger ($w/H \simeq 0.07$ at the beam centre) when the velocity ratio is unity which is the initial velocity distribution required for a pure third modal response according to a rigid-plastic theory based on infinitesimal displacements (Figure 2(c) of [1]). The JET 3C computer program was also used to obtain the response of the same beam with an initial velocity amplitude ratio of 0.978 which gave rise to the first modal vibrations with an amplitude of $w/H \simeq 0.10$ at the beam center.

The theoretical methods developed in Reference [1] and herein disregard any in-plane or axial displacements as is customary for this type of problem. However, it turns out that the in-plane displacements (u) predicted by the numerical elastic-plastic method are generally one order of magnitude smaller than the associated lateral or transverse displacements (w) as shown in Table 3.

The energy ratio (E_r) for a beam is defined in Reference [1] as the ratio between the initial kinetic energy (K.E.) and the maximum possible amount of strain energy (S.E.) which can be absorbed by a beam in a wholly elastic manner. The maximum elastic strain energy is estimated for the present problem by simply multiplying the volume of material by $\sigma_o \varepsilon_o/2$ where $\varepsilon_o = \sigma_o/E$. The temporal variations of the total plastic work, total elastic strain energy (S.E.) and total kinetic energy (K.E.) in a beam according to the JET 3C numerical procedure are shown in Figure 10 for three different cases. One suitable energy ratio for the numerical results is given by the ratio of the initial kinetic energy to the maximum residual elastic strain energy when plastic flow ceases. In this circumstance, the energy ratios turn out to be 13.3, 24.5 and 46.6 for the beams examined in Figures 10(a) to 10(c), whereas the corresponding values of E_r given by equation (44) in Reference [1] are 2.01, 5.24 and 5.56, respectively. This confirms, at least for these particular cases, that the general procedure for calculating energy ratios developed in the Appendix of Reference [1] and specialized to the present problem in Reference [1] is conservative.

6. Conclusions.

The higher modal dynamic plastic response of fully clamped beams has been examined using various rigid perfectly plastic theoretical procedures and a numerical elastic-plastic computer code. The theoretical predictions of equation (72), which retains the influence of geometry changes, and the numerical results agree reasonably well with the corresponding experimental values on strain rate insensitive beams which were subjected to first and second modal initial velocity distributions. However, all the experimental results for the third mode case lie below the various theoretical methods and numerical results, the reason for which is possibly due to the neglect of transverse shear effects.

Acknowledgements.

The work reported herein was supported by the Structural Mechanics Program of O.N.R. (current contract number N00014-76-C-0195, Task NR 064-510) and the Solid Mechanics Program of N.S.F. (current grant number ENG 75-13642). The authors also wish to take this opportunity to express their appreciation to Professor E.A. Witmer and Mr. H. L. M. Reis for their kind cooperation and assistance with the numerical calculations.

References.

1. N. Jones and T. Wierzbicki, A Study of the Higher Modal Dynamic Plastic Response of Beams, Int. J. Mech. Sci., In Press.

2. N. Jones, A Literature Review of the Dynamic Plastic Response of Structures, The Shock and Vibration Digest, 7, No8, 89-105 (1975).

3. N. Jones, A theoretical Study of the Dynamic Plastic Behavior of Beams and Plates with Finite-Deflections, Int.J.Solids and Structures, 7, 1007-1029 (1971).

4. R.W.-H. Wu and E.A. Witmer, Computer Program - JET3 to calculate the Large Elastic-Plastic Dynamically-Induced Deformations of Free and Restrained,Partial and/or Complete Structural Rings, NASA Tech. Rep. CR-120993 (1972).

5. R.W.-H. Wu and E.A. Witmer, Nonlinear Transient Responses of Structures by the Spatial Finite-Element Method, AIAA Journal, 11, 1110-1117 (1973).

6. M. Taya and T. Mura, Dynamic Plastic Behavior of Structures Under Impact Loading Investigated by the Extended Hamilton's Principle, Int. J. Solids and Structures, 10, 197-209 (1974).

7. S. R. Bodner, Strain Rate Effects in Dynamic Loading of Structures, Behavior of Materials Under Dynamic Loading, N. J. Huffington (ed.) ASME, 93- 105 (1965).

8. P.S. Symonds, Survey of Methods of Analysis for Plastic Deformation of Structures Under Dynamic Loading, Brown Univ. Rep. BU/NSRDC/ 1-67 (1967).

9. P. S. Symonds, Plastic Shear Deformations in Dynamic Load Problems, Engineering Plasticity, Eds. J. Heyman and F.A.Leckie, C.U.P. 647-664 (1968).

10. N. Jones, Dynamic Behavior of Ideal Fibre-Reinforced Rigid-Plastic Beams, J. App. Mechs., 43, 319-324 (1976).

11. N. Jones, J.W. Dumas, J.G. Giannotti and K.E. Grassit, The Dynamic Plastic Behavior of Shells, Dynamic Response of Structures, G. Herrmann and N. Perrone (eds). Pergamon Press, 1-29 (1972).

List of Tables.

MODE	SPECIMEN NUMBER [1]	x (in)	t (μsec)	$\frac{Q}{Q_o}$
1	6	1.00	40.4	0.13
		0.25	121.3	0.16
		0.25	141.5	0.17
2	11	0.25	20.2	0.21
		0.25	40.5	0.24
		0.50	40.5	0.17
3	23	0.10	20.3	0.35
		0.10	60.9	0.25
		0.30	60.9	0.25

TABLE 1

MODE	SPECIMEN NUMBER [1]	x (in)	t (μsec)	TOTAL AXIAL STRAIN	
				LOWER SURFACE	UPPER SURFACE
1	6	0.125	101	-0.021	0.043
		0.125	182	-0.030	0.065*
		0.125	647	-0.026	0.053
		0.375	647	-0.0008	0.003
2	11	1.375	61	0.066	-0.026
		0.125	101	-0.039	0.095*
		0.125	465	-0.033	0.074
		1.375	465	0.055	-0.022
3	23	0.050	61	-0.084	0.167*
		1.050	61	0.121	-0.056
		2.450	61	-0.057	0.122
		0.050	996	-0.078	0.146

TABLE 2

MODE	SPECIMEN NUMBER [1]	x (in)	t (μsec)	$\frac{u}{w}$
1	6	1.75	20.2	-0.0021
		2.00	80.8	-0.0078
		1.75	181.9	-0.0150
2	11	0.25	60.7	0.1992
		1.75	60.7	0.0653
		1.75	80.9	0.0691
3	23	0.20	81.3	0.1462
		1.20	81.3	0.0770
		2.20	81.3	0.0555

TABLE 3.

List of Figures

Figure 6. Maximum permanent transverse deflections of fully clamped beams subjected to initial velocity fields with a third modal shape.

The various curves are defined in the title of Figure 4.

o,● experimental test results recorded at center and outer zones, respectively, and given in Table 3 of Reference [1] .

$+^L$, $+^c$ numerical elastic-plastic predictions of JET3C for specimen number 22 in Table 3 of Reference [1] with $\lambda = 31.5$ (25 elements/half span, time step = 0.1016 μsec). L and c refer to the outer and central zones of the beam.

o^L, o^c numerical elastic-plastic prediction of JET3C for the beam described in the title of Figure 8.

Figure 7. Transverse displacement-time histories according to JET3C computer program with a central-difference temporal operator and 10 finite-elements/half span.

(a) First mode. Parameters for specimen number 6 in Table 1 of Reference [1] with $\lambda = 17.82$ (time step = 0.2526 μsec).

— — — estimated permanent transverse displacement at beam cent

—•—•— experimental value of maximum permanent transverse deflection of specimen number 6 in Table 1 of Reference [1] .

(b) Second mode. Parameters for specimen number 11 in Table 2 of Reference [1] with $\lambda = 46.6$ (time step = 0.2529 μsec).

— — — — estimated permanent transverse displacement at x = 1.50 in. from support. The node at x = 1.50 in. is the one nearest to η_1 = 1.47 in.

—•— • — experimental values for maximum permanent transverse deflections of specimen number 11 in Table 2 of Reference [1] .

Figure 8. Transverse displacement-time history for the third mode test specimen number 23 in Table 3 of Reference [1] according to JET3C computer program with $\lambda = 48.13$ (Central-difference temporal operator, time step = 0.1016 μsec, 25 finite-elements/ half span).

_____ transverse displacement at center.

---------- transverse displacement at x = 1.00 in from support. This displacement is actually negative, but is plotted positive for convenience. The node at x = 1.0 in is the one nearest to $\eta_1 = 1.039$ in.

-------1 estimated permanent transverse displacement at x = 1.0 in.

_____2 estimated permanent transverse displacement at beam center.

Figure 9. Comparison of experimental permanently deformed profiles and transverse deflections predicted by various theoretical methods.

(a) First mode. Specimen number 6 in Table 1 of Reference [1] .

_____ experimental results

— - — - equation (72) with $\lambda = 17.7$.

— — — equation (72) with σ_o replaced by $0.618\sigma_o$ and $\lambda = 17.7$.

+,o numerical elastic-plastic predictions of JET3C computer program for beam described in the title of Figure 7(a) at t = 1314 μsec and 1556 μsec, respectively.

(b) Second mode. Specimen number 11 in Table 2 of Reference [1] .

_____ experimental results.

_ _ _ _ _ equation (72) with $\lambda = 45.99$

_ _ _ _ _ _ _ equation (72) with σ_o replaced by $0.618\sigma_o$ and $\lambda = 45.99$.

o, + numerical elastic-plastic predictions of JET3C computer program for beam described in the title of Figure 7(b) at t = 506 μsec and t = 587 μsec, respectively.

(c) Third mode. Specimen number 23 in Table 3 of Reference [1].

_____ experimental results.

_ _ _ _ _ _ equation (72) with $\lambda = 48.13$

---------- equation (72) with σ_o replaced by $0.618\sigma_o$ and $\lambda = 48.13$.

o, + numerical elastic-plastic predictions of JET 3C computer program for beam described in title of Figure 8 at t = 1077 μsec and t = 1382 μsec, respectively.

Figure 10. Temporal variation of plastic work, elastic strain energy (S.E.) and kinetic energy (K.E.) for (a) first mode, (b) second mode and (c) third mode test specimens described in the titles of Figures 7(a), 7(b) and 8, respectively. (R = 1 is total initial kinetic energy).

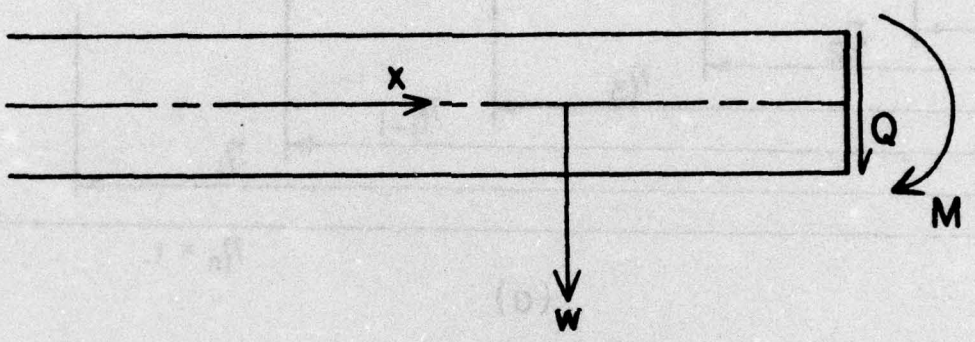

FIGURE 1

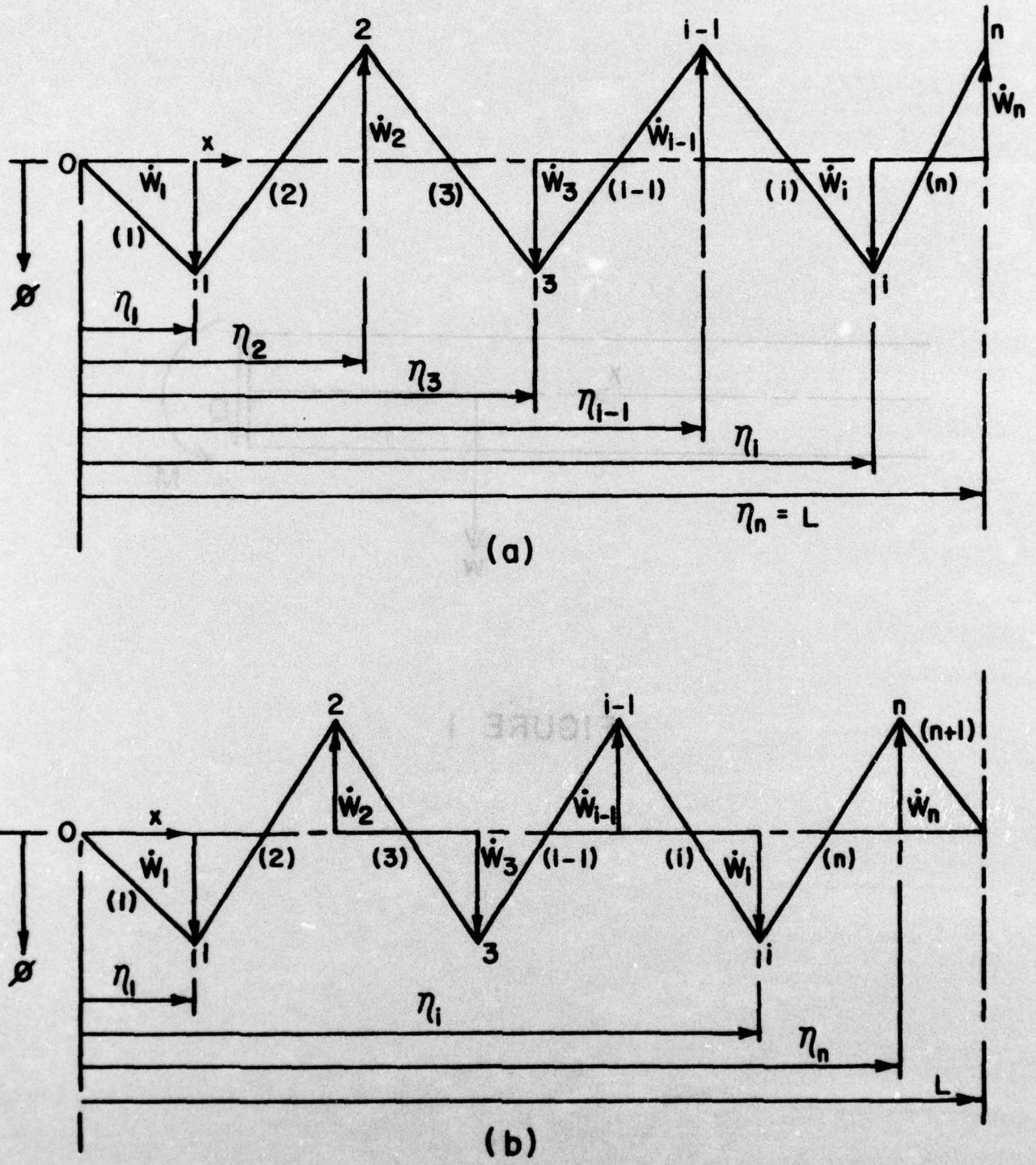
2
i-1
n
$\dot{W}_n$
$\dot{W}_2$
$\dot{W}_{i-1}$
x
0
$\dot{W}_1$
(2)
(3)
$\dot{W}_3$
(i-1)
(i)
$\dot{W}_i$
(n)
(1)
1
3
i
η_1
η_2
η_3
η_{i-1}
η_i
$\eta_n = L$
(a)
2
i-1
n
(n+1)
$\dot{W}_2$
$\dot{W}_{i-1}$
$\dot{W}_n$
x
0
$\dot{W}_1$
(2)
(3)
$\dot{W}_3$
(i-1)
(i)
$\dot{W}_i$
(n)
(1)
1
3
i
η_1
η_i
η_n
L
(b)

FIGURE 2

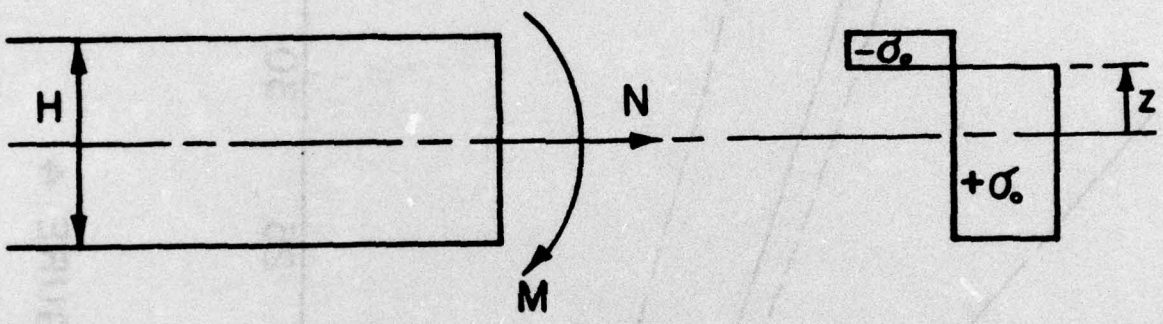

FIGURE 3

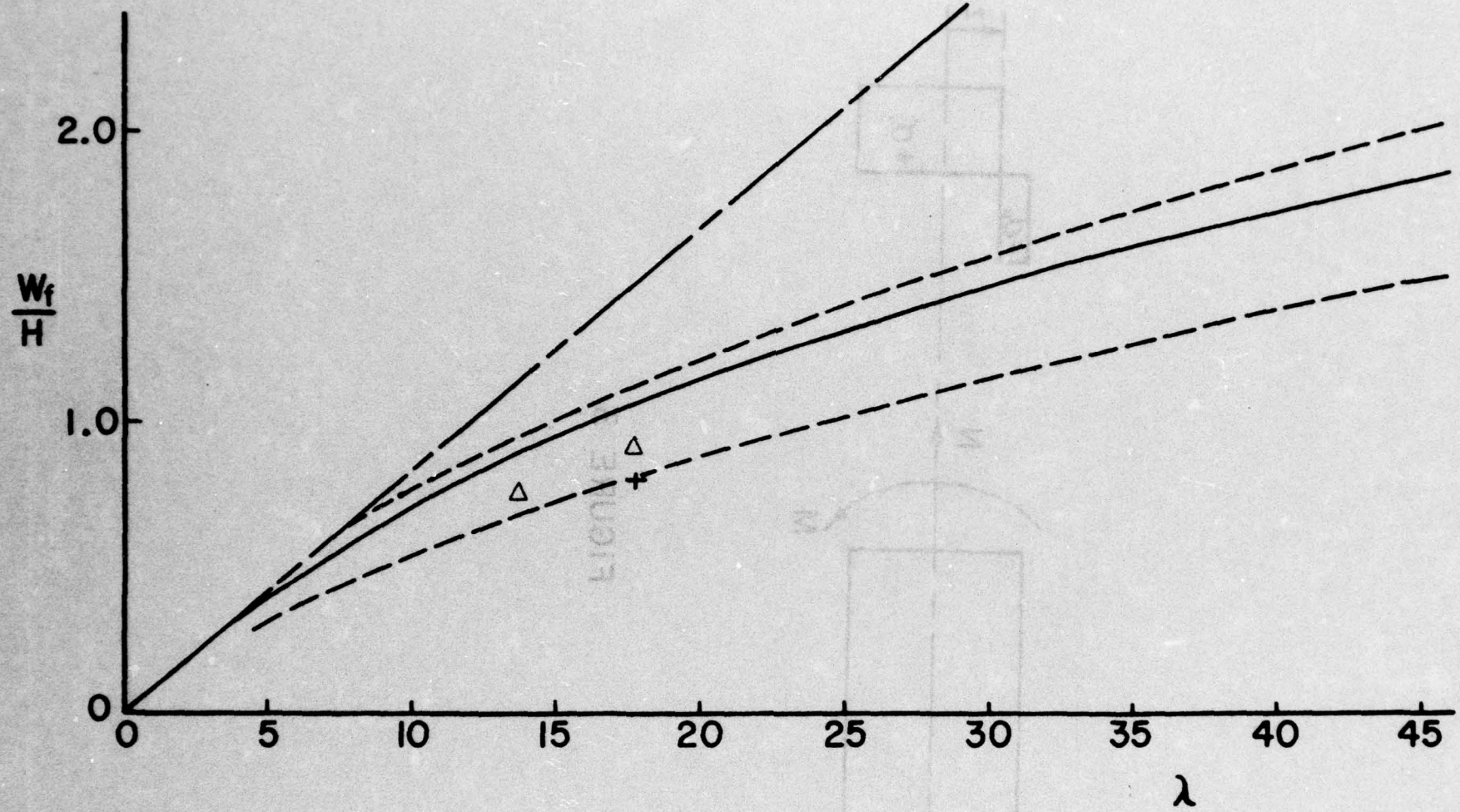

FIGURE 4

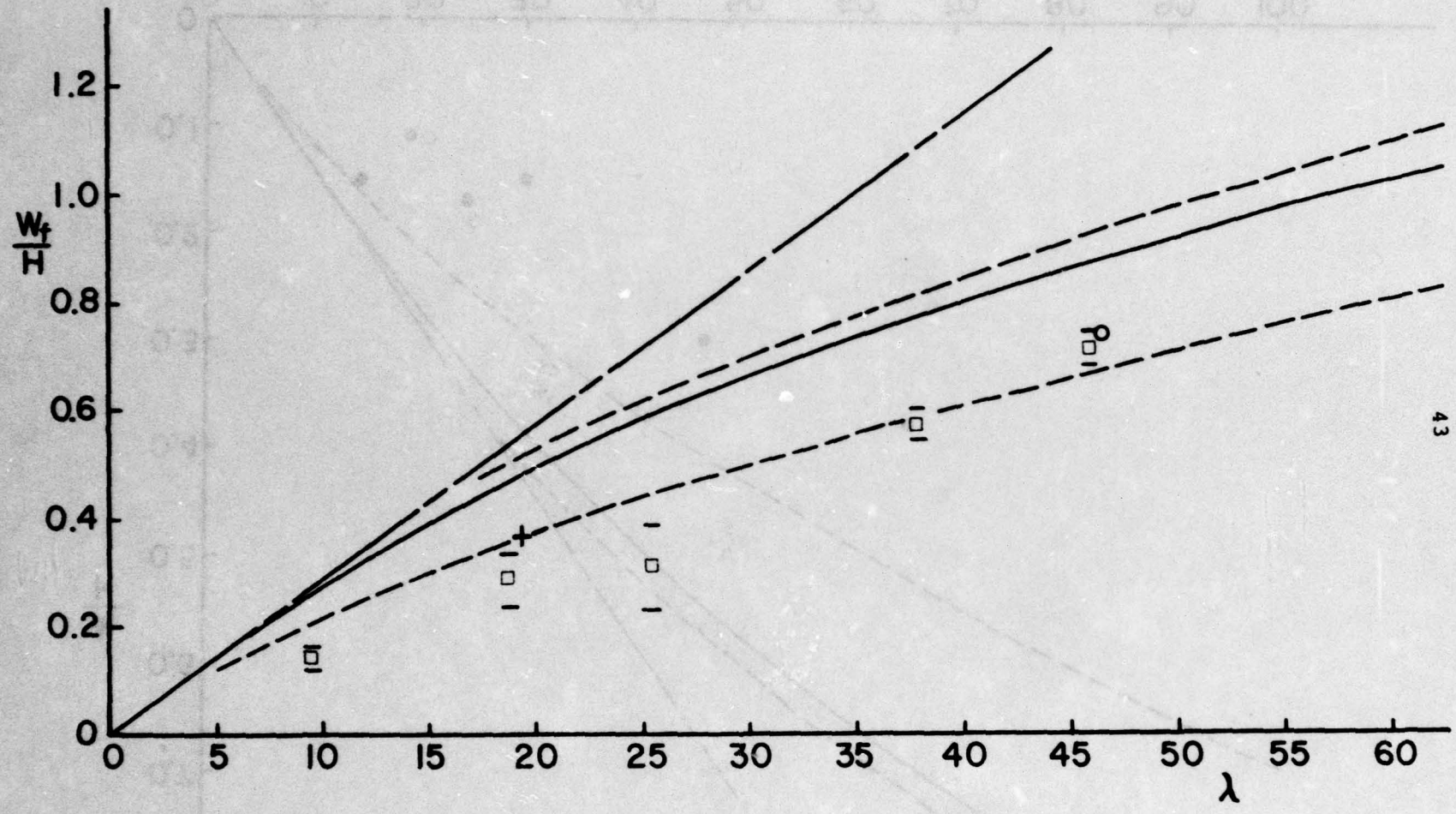

FIGURE 5

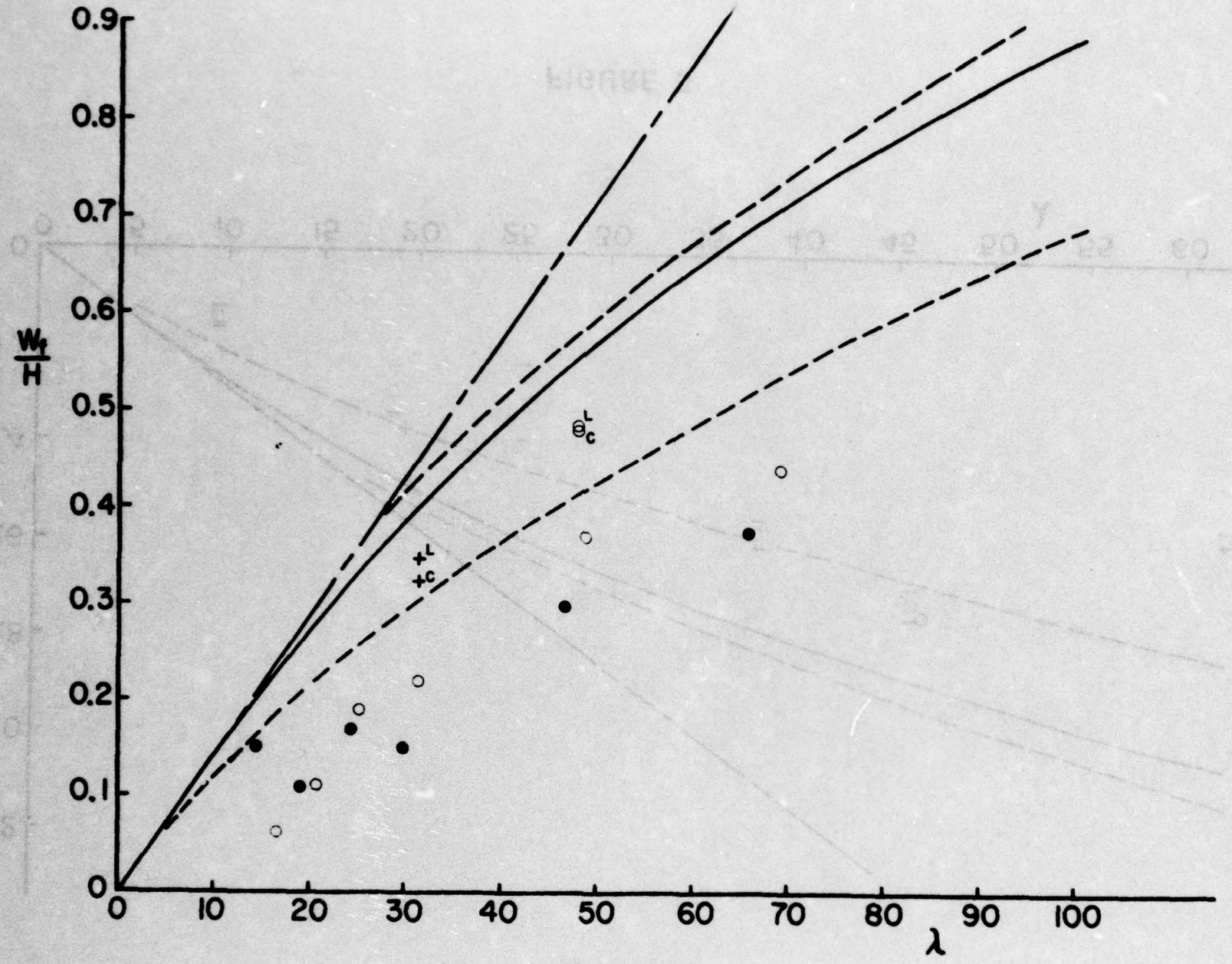
0.9
0.8
0.7
0.6
0.5
0.4
0.3
0.2
0.1
0
$\frac{W_f}{H}$
θ_c^L
$+^L_{+c}$
0
10
20
30
40
50
60
70
80
90
100
λ

FIGURE 6

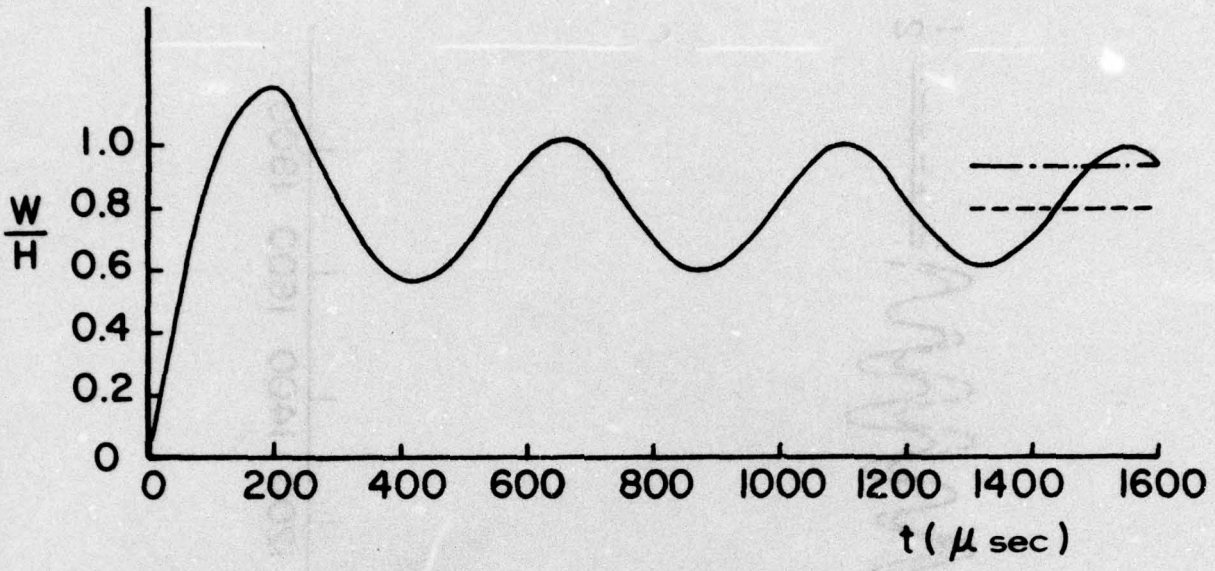
W/H
1.0
0.8
0.6
0.4
0.2
0
0
200
400
600
800
1000
1200
1400
1600
t (μ sec)

(a)

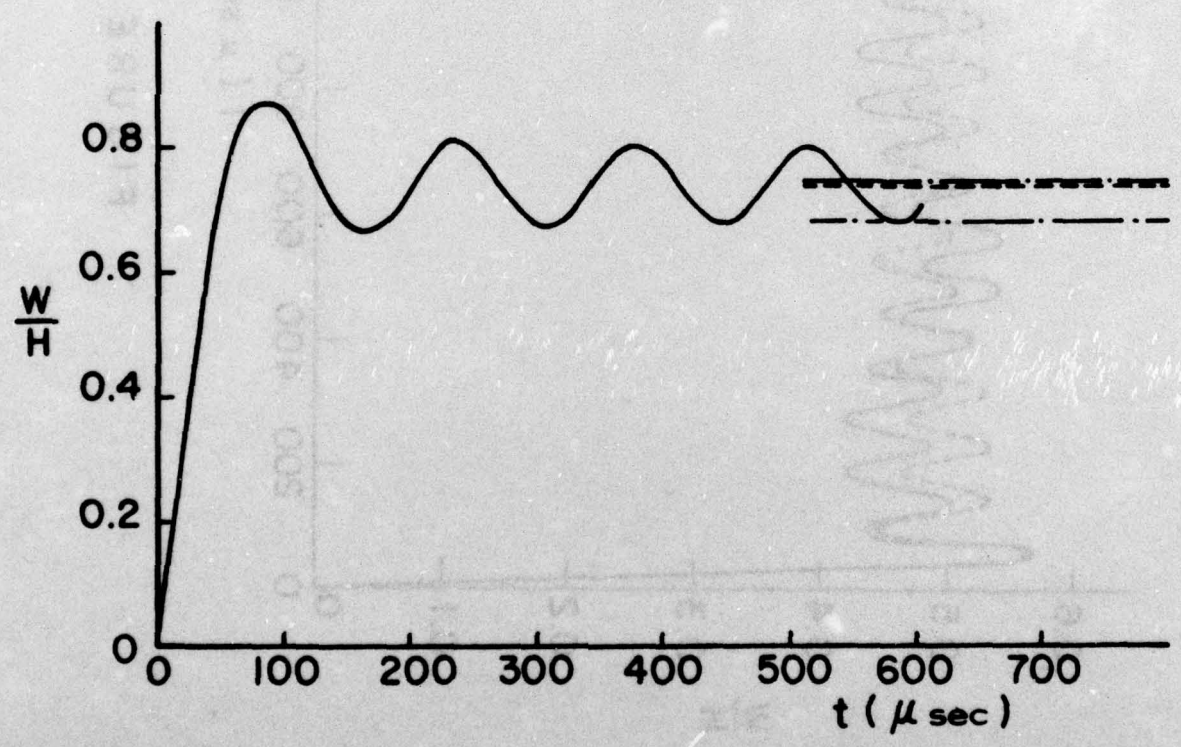
W/H
0.8
0.6
0.4
0.2
0
0
100
200
300
400
500
600
700
t (μ sec)

(b)

FIGURE 7

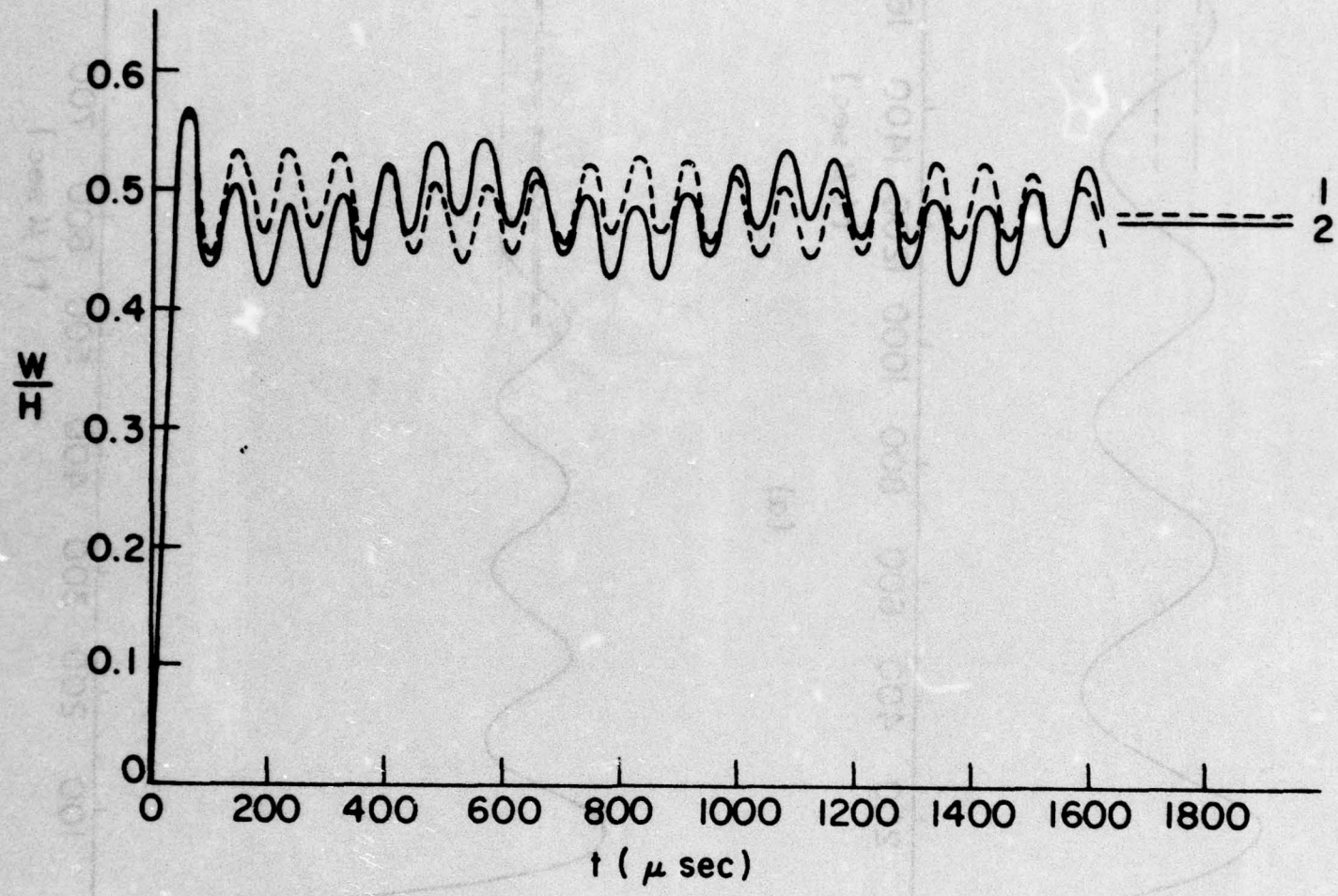
0.6
0.5
0.4
0.3
0.2
0.1
0
W/H
1/2
0
200
400
600
800
1000
1200
1400
1600
1800
t (μ sec)

FIGURE 8

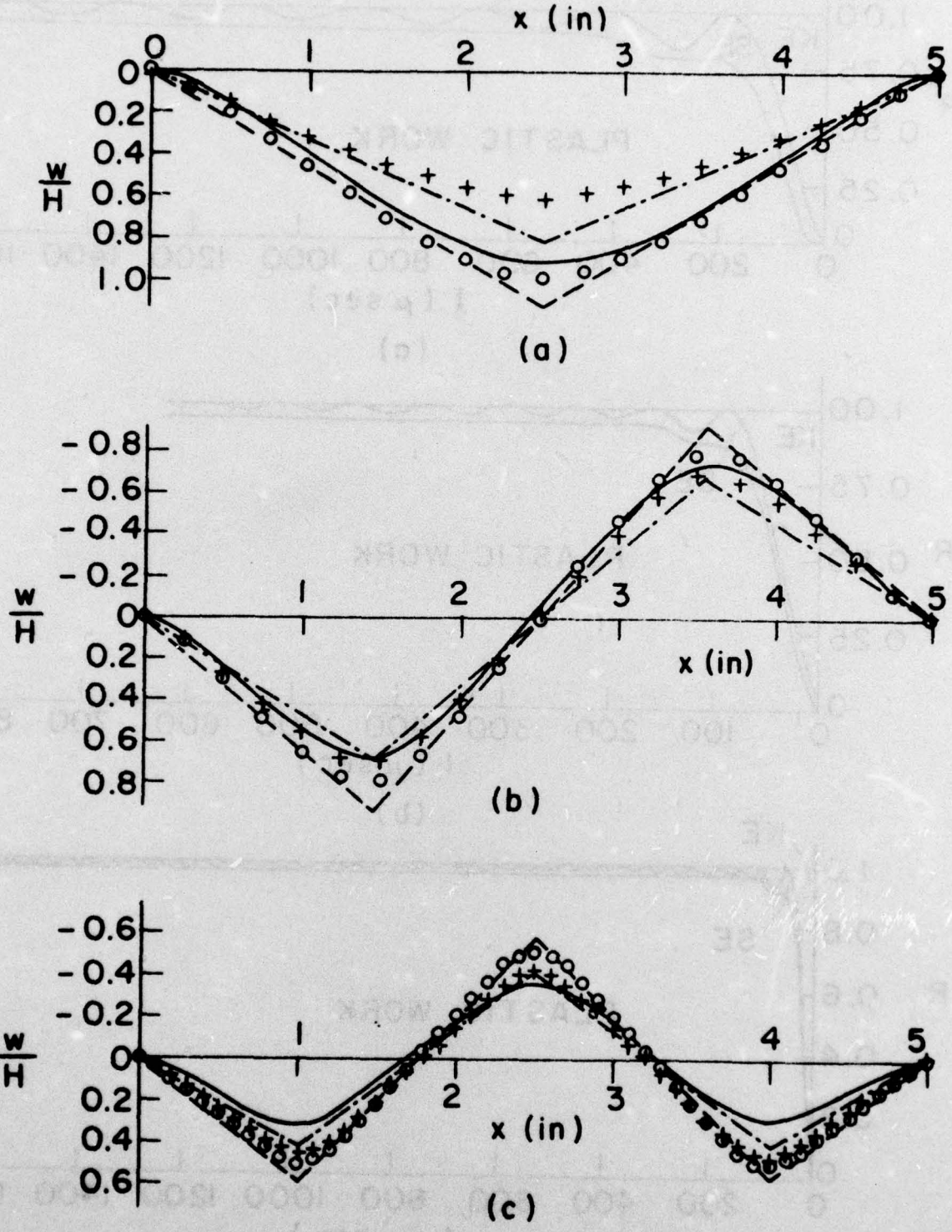
x (in)
0
1
2
3
4
5
0
0.2
0.4
0.6
0.8
1.0
w/H
(a)
-0.8
-0.6
-0.4
-0.2
0
0.2
0.4
0.6
0.8
w/H
x (in)
(b)
-0.6
-0.4
-0.2
0
0.2
0.4
0.6
w/H
x (in)
(c)

FIGURE 9

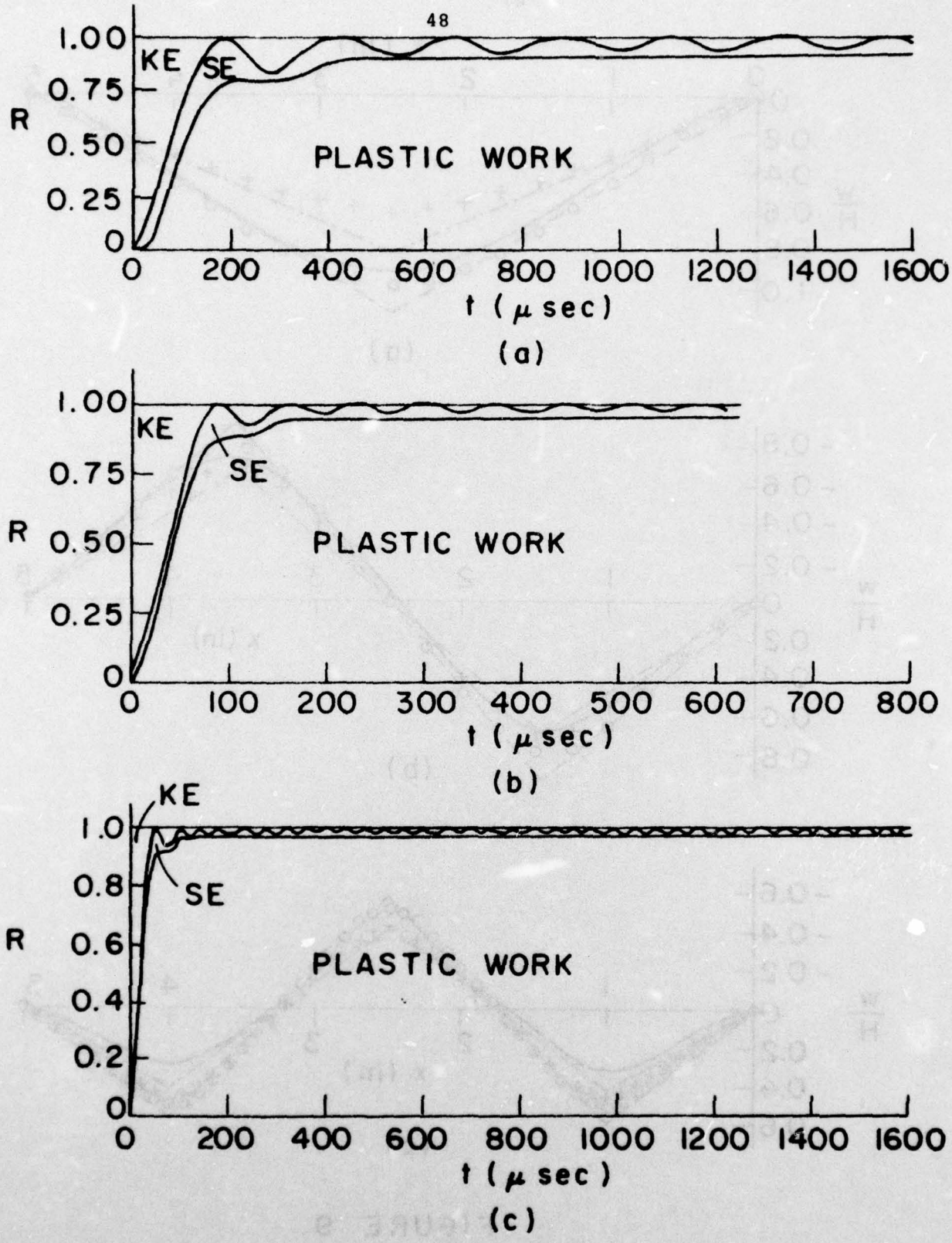
1.00
0.75
0.50
0.25
0
R
KE
SE
PLASTIC WORK
0
200
400
600
800
1000
1200
1400
1600
t (μ sec)
(a)
1.00
0.75
0.50
0.25
0
R
KE
SE
PLASTIC WORK
0
100
200
300
400
500
600
700
800
t (μ sec)
(b)
KE
1.0
0.8
0.6
0.4
0.2
0
R
SE
PLASTIC WORK
0
200
400
600
800
1000
1200
1400
1600
t (μ sec)
(c)

FIGURE 10

UNCLASSIFIED

SECURITY CLASSIFICATION OF THIS PAGE (When Data Entered)

REPORT DOCUMENTATION PAGE	READ INSTRUCTIONS BEFORE COMPLETING FORM
1. REPORT NUMBER (14) 76-5	2. GOVT ACCESSION NO.
3. RECIPIENT'S CATALOG NUMBER (9)	
4. TITLE (and Subtitle) (6) HIGHER MODAL DYNAMIC PLASTIC BEHAVIOR OF BEAMS LOADED IMPULSIVELY.	5. TYPE OF REPORT & PERIOD COVERED Interim rept.,
6. PERFORMING ORG. REPORT NUMBER 76-5	
7. AUTHOR(s) (10) Norman Jones C.A.P. Guedes Soares	8. CONTRACT OR GRANT NUMBER(s) (15) N0014-76-C-0195 Task NR 064-510
9. PERFORMING ORGANIZATION NAME AND ADDRESS Department of Ocean Engineering Massachusetts Institute of Technology Cambridge, Massachusetts 02139	10. PROGRAM ELEMENT, PROJECT, TASK AREA & WORK UNIT NUMBERS
11. CONTROLLING OFFICE NAME AND ADDRESS (11) Structural Mechanics Program O.N.R., Arlington, Virginia 22217	12. REPORT DATE October 1976 13. NUMBER OF PAGES 48
14. MONITORING AGENCY NAME & ADDRESS (if different from Controlling Office) (12) 56p.	15. SECURITY CLASS. (of this report) Unclassified 15a. DECLASSIFICATION/DOWNGRADING SCHEDULE
16. DISTRIBUTION STATEMENT (of this Report) Unlimited distribution	
17. DISTRIBUTION STATEMENT (of the abstract entered in Block 20, if different from Report)	
18. SUPPLEMENTARY NOTES	
19. KEY WORDS (Continue on reverse side if necessary and identify by block number) DYNAMIC PLASTIC BEAMS MODES	

20. ABSTRACT (Continue on reverse side if necessary and identify by block number)

The higher modal dynamic plastic response of fully clamped beams has been examined using various rigid perfectly plastic theoretical procedures and a numerical elastic-plastic computer code. The theoretical predictions of equation (72), which retains the influence of geometry changes, and the numerical results agree reasonably well with the corresponding experimental values on strain rate insensitive beams which were subjected to first

→ next page

DD FORM 1 JAN 73 1473 EDITION OF 1 NOV 65 IS OBSOLETE
S/N 0102-014-6601

UNCLASSIFIED

SECURITY CLASSIFICATION OF THIS PAGE (When Data Entered)

406856 LB

Continuation of Box 20 on front side

cont.

and second modal initial velocity distributions. However, all the experimental results for the third mode case lie below the various theoretical methods and numerical results, the reason for which is possibly due to the neglect of transverse shear effects.